



This is the accepted manuscript made available via CHORUS. The article has been published as:

Large and tunable spin-orbit effect of math xmlns="http://www.w3.org/1998/Math/MathML">mrow>mn >6/mn>mi>p/mi>/mrow>/math> orbitals through structural cavities in crystals

Mauro Fava, William Lafargue-Dit-Hauret, Aldo H. Romero, and Eric Bousquet Phys. Rev. B **108**, L201112 — Published 14 November 2023

DOI: 10.1103/PhysRevB.108.L201112

Large and tunable spin-orbit effect of 6p orbitals through structural cavities in crystals

Mauro Fava, William Lafargue-Dit-Hauret, Aldo H Romero, and Eric Bousquet

1 Physique Théorique des Matériaux, QMAT, CESAM,
Université de Liège, B-4000 Sart-Tilman, Belgium

2 Universite de Pau et des Pays de l'Adour, E2S UPPA, CNRS, IPREM, Pau, France

3 Department of Physics and Astronomy, West Virginia University, Morgantown, WV 26505-6315, USA
(Dated: October 27, 2023)

We explore from first-principles calculations the ferroelectric material $Pb_5Ge_3O_{11}$ as a model for controlling the spin-orbit interaction (SOC) in crystalline solids. The SOC has a surprisingly strong effect on the structural energy landscape by deepening the ferroelectric double well. We observe that this effect comes from a specific Pb Wyckoff site that lies on the verge of a natural cavity channel of the crystal. We also find that a unique cavity state is formed by the empty 6p states of another Pb site at the edge of the cavity channel. This cavity state exhibits a sizeable spin splitting with a mixed Rashba-Weyl character and a topologically protected crossing of the related bands. We also show that the ferroelectric properties and the significant SOC effects are exceptionally robust against n-doping up to several electrons per unit cell. We trace the provenance of these original effects to the unique combination of the structural cavity channel and the chemistry of the Pb atoms with 6p orbitals localizing inside the channel.

Relativistic atomic spin-orbit coupling (ASOC) was first introduced in the early 1930s during the development of quantum mechanics. It refers to the interaction between the electronic spin (S) and its angular momentum (L). Even though ASOC is weak compared with Coulomb or kinetic interactions (one to two orders of magnitude) and even weaker in molecules or crystals owing to the quenching of L with chemical bonding, it appears to be the fundamental interaction to describe, for example, the atomic magnetic moment directions (magnetic anisotropy), magnetostriction or spin canting, and weak ferromagnetism [1]. Hence, SOC has been a centerpiece of molecular and condensed matter physics, and a recent revival of interest is now at play with the discovery of new SOC-related phenomena like spin torques [2, 3], skyrmions [4-6], the presence of a topological \mathbb{Z}_2 order [7, 8], quantum spin-Hall effect [9–12], the existence of spin states with long lifetimes [13–17], linear [18–22] and cubic [23–25] Rashba (R) and Dresselhaus (D) spin splitting, and so on. These new phenomena are significant for future spintronic applications. The term spinorbitronics was also foreseen when the SOC is the driving ingredient [26].

Thus, controlling spin-orbital features is paramount for realizing numerous phenomena with high technological impact. On the other hand, finding a single material that encompasses several useful and significant SOC features and guarantees, as a matter of principle, a reasonable degree of handling over the "internal" parameters is difficult. Furthermore, concerning the Rashba physics, which requires doping to be harnessed in polar insulators, a known problem is the preservation of the mirror symmetry breaking in doping conditions since screening by free charges tends to destabilize the electric polarisation [27]. In this letter, we address both issues at once. We use the ferroelectric axial [28, 29] compound lead germanate oxide Pb₅Ge₃O₁₁ (PGO) [30, 31] as a single platform for the manipulation of spin-orbit inter-

action. We show from density functional theory (DFT) calculations (see supplementary information [32] and the references [33–40] therein included) that SOC has an unexpectedly significant impact on both the structural energy landscape of PGO and its electronic structure with a mixed Rashba-Weyl crossing between the spin bands, which is topologically protected by a Z₂ invariant. More specifically, we show that this significant SOC effect originates from two unique features: i) a vacuum channel in the crystal structure that localizes and unquenches the empty 6p orbitals of some specific lead cations, and ii) the breaking of the mirror site symmetry at other Pb sites. In addition, we show that, unlike common ferroelectric materials, the ferroelectric energy is enhanced by negative carrier doping, which we explain in terms of the short-range nature of the polar instability and localization of the aforementioned 6p states. From these results, we discuss the design rules for controlling spin-orbital features in solid materials.

PGO is a bandgap insulator that undergoes a ferroelectric structural phase transition at 450 K [30]. Hence, it is a room-temperature uniaxial ferroelectric (FE) and chiral material (P3 space group 143) with a measured spontaneous polarization of $\sim 5 \,\mu\text{C/cm}^{-2}$ along the c axis. The combination of chirality and ferroelectricity makes PGO gyroelectric and electrogyroelectric and the natural optical activity can be tuned and switched by an applied electric field following a hysteresis process [41, 42]. We provide a schematic view of the high-symmetry $P\bar{6}$ phase (space group 174) in Figure 1. The unit cell of PGO contains 57 atoms, and the PE (FE) phase is described by 15 (23) asymmetric Wyckoff positions (WP). The crystal structure can be described as follows. The germanium atoms either form - along with the surrounding oxygens - GeO_4 tetrahedra (z = 0.5, 6l WP) or Ge_2O_7 dimers (z = 0, 3k WP) The lead atoms bridged the Ge_2O_7 and GeO₄ units. Pb atoms can be separated into two groups. The first group of Pb atoms was located in 6l and 3k WP

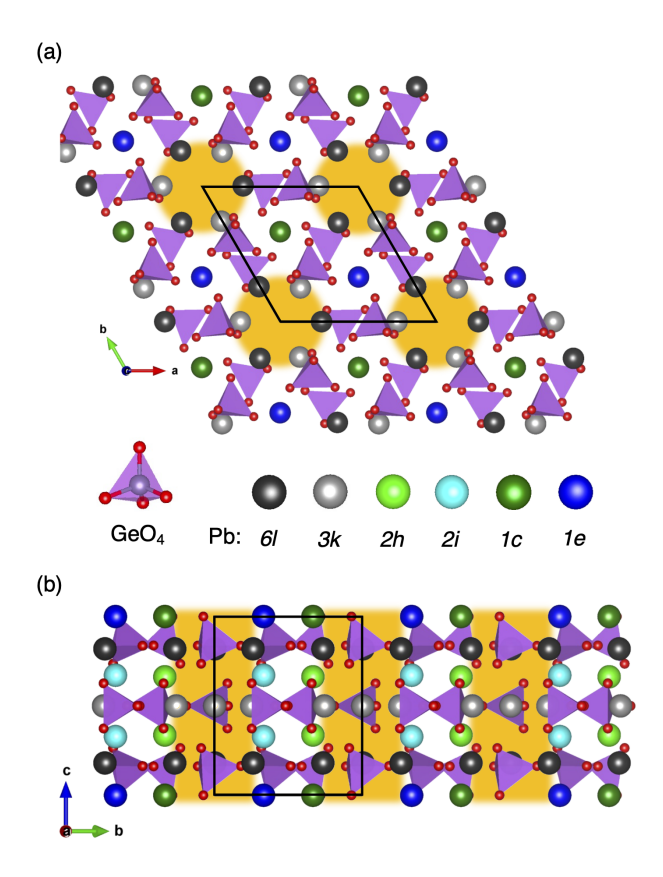


FIG. 1. Top (a) and side (b) view of PGO (PE phase). Oxygen atoms are shown in red, Ge atoms and germanate units in purple, while the lead ions are distinguished by their Wyckoff positions. Empty channels are evidenced in yellow.

(black and grey atoms in Figure 1) form empty hexagonal channels that propagate along the [001] crystallographic direction (highlighted in yellow in Figure 1). The second group consists of Pb atoms found between these channels, that is, the 1e, 1c, 2i, and 2h WP (dark blue, dark green, cyan, and lime atoms in Figure 1). Owing to the loss of mirror symmetry in the FE phase, the Pb-6l positions split into two pairs of 3d WPs (top and bottom unit cell) in the P3 phase.

We start by performing the optimisation of the lattice parameters, which are also in good agreement (see the supplementary file [32]) with their measured values ([30, 43, 44]). Defining $\Delta E=E(P\bar{6})$ - E(P3) as the energy gain between the paraelectric and the ferroelectric phase, we obtain $\Delta E(\text{no SOC})=68$ meV in the absence of SOC and $\Delta E(\text{with SOC})=89$ meV when the SOC is included in the calculation, i.e. an increase of 31%. This means that the ferroelectric double-well depth of PGO is strongly sensitive to the spin-orbit interaction. Furthermore, the SOC enhancement of ΔE is typically not as prominent in lead-based ferroelectrics such as PbTiO₃ [45]. Thus, these preliminary results call for a deeper investigation of the electronic properties to understand the significant effect of SOC on the ferroelectric well depth.

In Figure 2 (a), right panel, we report the spd projected

DOS around the last occupied valence state and the first unoccupied conduction state of the FE P3 phase. The top of the valence bands (VB) is dominated by O-2p states followed by contributions from the Pb-6s states and a small amount of Pb-6p states, suggesting sizable covalent hybridization between the oxygen and lead. The contributions from the d orbitals are almost absent because, as expected, both Ge and Pb d orbitals are far deeper in energy (approximately -10 eV). The conduction bands (CB) are dominated by the Pb-6p spectral weight and show a large Pb-6p/O-2p hybridization (plus the Pb-6s/O-2p in a smaller amount). In the left panel of Figure 2 (a), we report the electronic band structure of the P3 phase in the presence and absence of SOC. In the P3 (P6) phase without SOC we obtain a band gap of 2.48 (2.35) eV, which is reduced to 2.25 (2.11) eV if the SOC is included. It is shown in supplementary section that ΔE is negatively correlated with the gap size, experimentally found to be 3 eV [46, 47]. While SOC has only a small effect on the valence band maximum, which has mostly oxygen character, its impact on the CB is sizeable.

To better analyze and quantify the effect of spin-orbit interaction, we performed an irreducible representation (IR) analysis of the VB maximum (VBM) and CB minimum (CBM) states at the Γ point [32]. A scheme of SOC-induced splitting for P3 phase is highlighted in Figure 2(b). When the SOC is switched off, the top-VB is populated by states belonging to the invariant representation of either the C_{3h} or C_3 point groups, whereas the bottom-CB is constituted by p_x , p_y orbitals (E' and E single representations of C_{3h} and C_3 respectively), with a state belonging to the invariant representation IR (Γ_1) located higher in energy. With reference to the conduction bands in the P3 phase we define $\gamma = |E(\bar{\Gamma}_4) - E(D_{1/2})|$, with the split-off energy between the invariant and the p_x , p_y orbitals in the absence of SOC as its upper bound. Clearly, the ferroelectric phase transition does not affect the in-plane p-levels, and adding the spin-orbit results in additional splitting, which in the FE case can be defined as $\delta = |E(\bar{\Gamma}_5 \oplus \bar{\Gamma}_6) - E(\bar{\Gamma}_4)|$. From our calculations, we obtain $\delta = 180 \text{ meV}$, whereas γ is reduced from 270 meV (no SOC) to 106 meV (with SOC). Such a large SOC effect on the electronic band structure is approximately of the same order of magnitude as that of bulk Au [48], but it is unexpected for ferroelectric insulators with Pb²⁺ cations such as PbTiO₃ [45]. Contrarily to the case of halide perovskites like CsPbBr₃ [49], the singlet-triplet SOC-induced inversion does not occur.

In addition, the orbital angular momentum ${\bf L}$ over the Γ -CBM states is unquenched [32], which means that the SOC is a first-order correction $\sim \langle {\bf L} \rangle \cdot {\bf S}$ of the electronic energies as opposed to the case of the previously reported BiTeI [50]. We employed the ${\bf k} \cdot {\bf p}$ approximation near the Γ point to further understand the conduction band states. The high-symmetry phase has been explored in a previous study [51] therefore, we focus only on the ferroelectric phase. The details of our DFT-based results

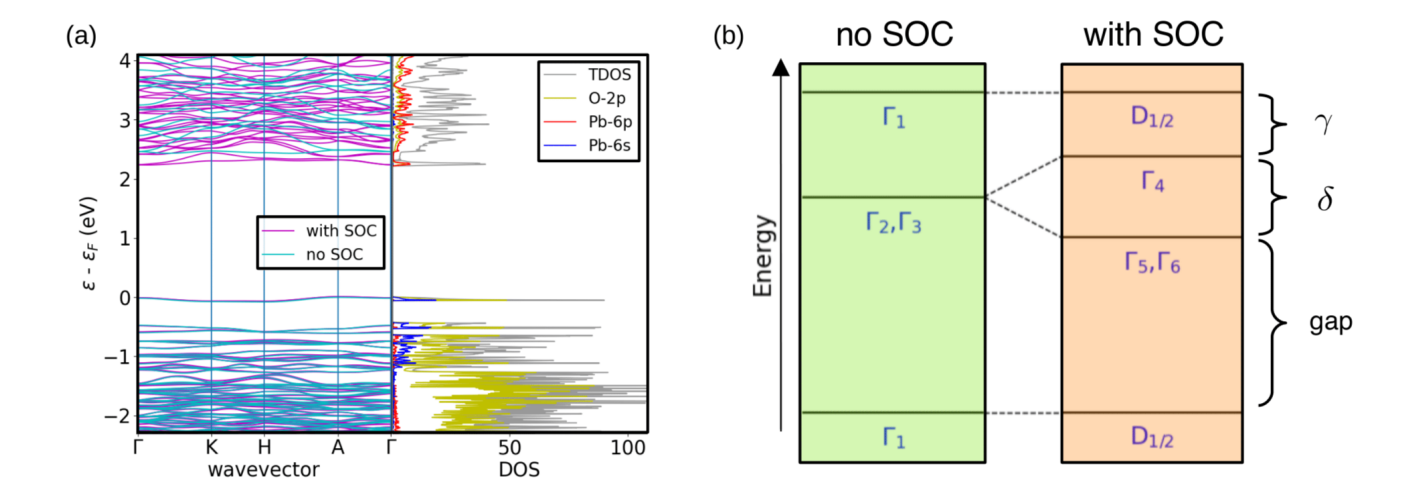


FIG. 2. (a) Band structure (left) and orbital-projected density of states (right) of the ferroelectric P3 phase. The SOC splitting is clearly evident in the conduction bands bottom. (b) A schematics of the spin-orbit induced splitting (single to double irreducible representation) of the CBM / VBM levels for the FE phase. The IR labels of the C_{3h} and C_3 point groups are the same as in the Bilbao Crystallographic Server, while D is the $SO(3) \times \{1, -1\}$ spin representation reduced to 3-fold rotations and the z-mirror inversion.

(both PE and FE cases) are reported in the supplement file [32] along with a discussion about the symmetry-induced protection of the spin state (see also the references [52–54] and [16, 55]). The spin-orbit part of the P3 phase ($\bar{\Gamma}_5 \oplus \bar{\Gamma}_6$) can be described by:

$$H_{\rm P3}^{\rm SOC}(\mathbf{k}) = \lambda_R(k_y\sigma_x - k_x\sigma_y) + \sum_{i=x,y,z} \lambda_{W_i}k_i\sigma_i,$$
 (1)

where λ_R (-0.10 eV·Å) is the Rashba interaction strength and where $\lambda_{W_x} = \lambda_{W_y} \equiv \lambda_w \ (0.11 \text{ eV-Å})$ and $\lambda_{W_z} \ (0.01 \text{ eV-Å})$ $eV\cdot \mathring{A})$ represents a Weyl-type band spin splitting, where σ labels the spin. We define $\alpha = \sqrt{\lambda_R^2 + \lambda_w^2} \; (0.15 \; \text{eV} \cdot \text{Å})$ to easily quantify the SOC strength. The values of the SOC parameters is comparable with those of Bi₂WO₆, BiAlO₃, GeTe or BiTeI (Ref. [27]), and it is one order of magnitude larger than the values reported in a recent work on LaAlO₃/LaFeO₃/SrTiO₃ [56]. Furthermore, exploiting the SOC in this material can be achieved without the need to engineer the unit cell, as it may occur with certain tungsten oxide compounds such as WO₃, which requires confinement in the direction perpendicular to the polarization [27]. The symmetries of the P3 space group allow for an electric field switchable [17] momentum-dependent [32, 57] spin texture and because polar domains of PGO are optically active, this suggests the possibility of controlling the handedness of the spin texture with chiral light. It is likely that an electric bias could also be used to tune λ_R , whereas at the same time a magnetic Zeeman interaction may be employed to displace but not remove the crossing between the spin bands. In particular, we realize [32] that this crossing is protected [58, 59] by a \mathbb{Z}_2 topological number because of the presence of a Weyl point at Γ , which means that the degeneracy of the spin cannot be removed by a magnetic

field.

We are left with the need for a microscopic explanation of the large SOC effects. We have seen that SOC mainly affects the conduction bands owing to its predominant Pb-6p character. To gain further insight, we show in Figure 3 the band projected charge density corresponding to the top-VB and bottom-CB isolated bands in the P3 phase. We find that the top valence electrons are mainly localized at the Pb-1c site and the oxygen 6l sites (sp hybridization), the latter bonding with the Ge₂O₇ units and Pb-1c and Pb-2h atoms. This localization near the Ge₂O₇ dimers is due to the Pb-6s states associated with the steep DOS peak at the Fermi level, which corresponds to 1c WP. On the other hand, the bottom CB charge (where SOC splitting is the most apparent with Pb-6p character) is found to be mostly localized in the vacuum channel and it comes from the Pb-6l WP that are around the cavity. It is striking to see in Figure 3 that this CB of the Pb-6l sites forms a unique and complex cavity state that is quite different from the atomic 6p orbital shapes. It is also interesting to notice that this cavity state exhibits large SOC features due to its cavity localization and unquenched L. We further highlight the presence of this phenomenon - independent from any mirror operation - in the $P\bar{6}$ phase as well [32].

To scrutinize the origin of the large SOC observed in PGO, we performed computer experiments by switching the SOC on and off on selected orbitals and at selected atomic sites. For each case, we recalculated the ferroelectric double-well depth ΔE and several SOC-related parameters of interest (including the aforementioned δ , γ and α) and band gap. The results are reported in tabs. III and IV of the supplementary materials [32]. This also indicates that the relatively small hybridiza-

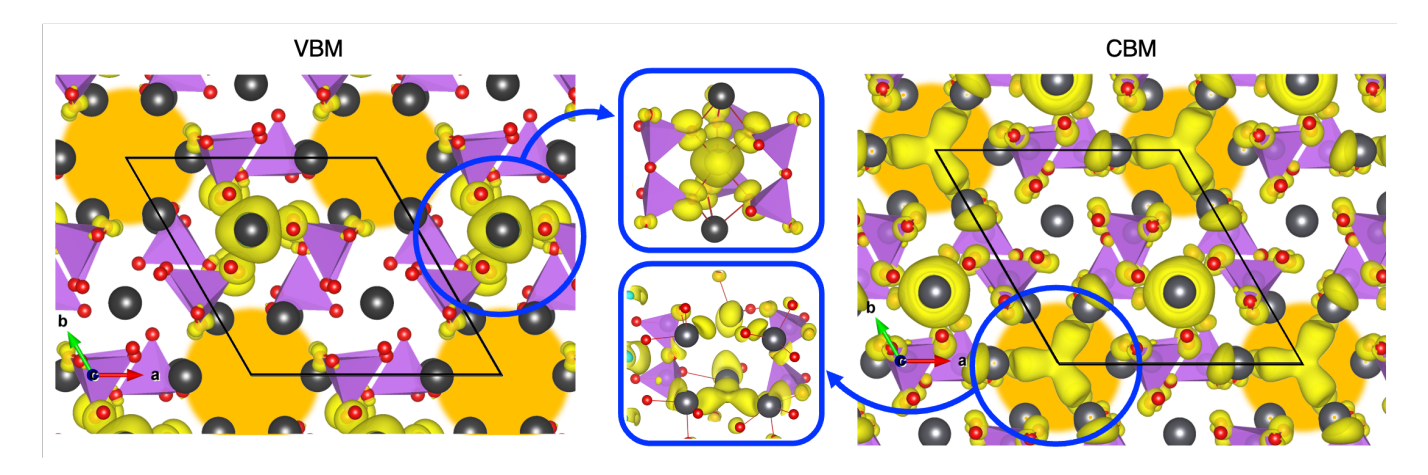


FIG. 3. Ferroelectric partial charge density associated with the VBM (iso = 0.001) and CBM (iso = 0.0005) energy windows states (PDOS peaks in Figure 2). Lead and oxygen atoms are shown in black and red respectively. GeO₄ tetrahedra are shown in purple, and empty channels are evidenced in gold.

tion of the Pb-6p states with Pb-6s/O-2p is responsible for the SOC renormalization of the energy landscape, as the empty states (CB) do not contribute to the energy. It also explains the aforementioned negative correlation of ΔE with the gap size. Now, for the six different Pb WP of the $P\bar{6}$ phase, we observe that deactivating the SOC at the 3k sites significantly affects the PE-FE energy barrier $(\sim 17 \% \text{ decrease}) \text{ compared to the } 6l, 1c, 1e, 2i \text{ and } 2h$ WPs ($<\sim 7\%$ variation). A reason for this - along with the aforementioned Pb-O interaction - can be attributed to the fact that the site symmetry group associated with the 3k WPs is m, which is broken by the phase transition, while the site symmetries induced by the other Pb positions are preserved. On the other hand, the spinsplitting and split-off CB parameters do not necessarily follow this trend because deactivating the SOC at 1c, 1e, 2i sites can produce a 2 or 3 times increase in the α parameter (for example, $\Delta E = 87 \text{ meV}$ and $\alpha = 2.9 \text{ eV} \cdot \text{Å}$ in the 2i-off case). Overall, the substitution (alloying) at the selected WP could either affect the ferroelectric domain barrier and/or the CB parameters (spin and band splitting) in a broad fashion, provided that further lowering of the symmetry (if present) and chemical changes have a small impact on the electronic states.

Finally, we discuss the robustness of the phase transition under doping. Exploiting the Rashba phenomenology requires, on the one hand, the breaking of the inversion symmetry and, on the other hand, the presence of free carriers, which tend to screen long-range forces responsible for polar instability [27, 60] and thus reduce the magnitude of the spin-splitting parameters. We have thus introduced some charge in the unit cell and performed the relaxation of the atomic positions, without relaxing the cell parameters at the same time (as the internal pressure is not well defined for charged systems in periodic boundary conditions [61]). Then we have calculated ΔE as a function of p and n carrier doping concentrations (see Figure 4). Contrary to regular ferroelectrics [60], ΔE is

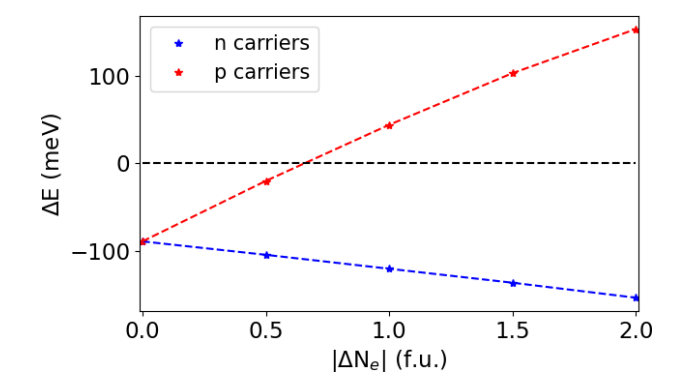


FIG. 4. $\Delta E = E(FE)$ - E(PE) as a function of extra n and p charge. While an increasing negative carrier concentration lowers the P3 phase energy even further with respect to the paraelectric case, the P $\bar{6}$ phase can be stabilised instead with a hole concentration above ~ 0.655 f.u..

surprisingly enhanced by n-doping of the CBM states. The calculation [62–64] of the phonons reveals [32] that the polar instability has a short-range origin. Hence, the screening of the Coulomb interaction by charges does not affect the instability, as in BaTiO₃ [62]. However, depopulating the VBM (p doping) can stabilize the paraelectric phase above a concentration of ~ 0.66 holes f.u., which highlights the importance of the VBM Pb-6s orbitals for the stabilization of the P3 phase. Finally, we find that the ferroelectric phase is further stabilised in the n-doping (plus one electron) scenario when the spin polarisation is included [32]. The extra electron localises inside the Pb-6p cavity states (fig. 9 of [32]) and possesses a magnetic moment which could be analysed in photoexcitation experiments. Moreover, the localisation of these states could provide the necessary coherence for qubit manipulation, also to be probed in future experimental works.

In conclusion, we have shown that the ferroelectric mate-

rial Pb₅Ge₃O₁₁ can be used as a single platform for controlling diverse spin-orbital properties. We find a large SOC-induced renormalization of ferroelectric double well. which originates from the O-2p/Pb-6p overlap along with the breaking of the mirror site symmetry at the Pb-3kpositions. Symmetry analysis shows that the FE structure leads to mixed Rashba-Weyl spin-splitting with Z₂ topological protection. We argue that the asymmetric localization of the 6p states inside the cavity channel, along with the large Z-number of Pb and first-order nature of the SOC energy correction, can produce large spin-orbital effects. The deactivation of the SOC at selected WPs also reveals a wide degree of control over the domain barrier and conduction band parameters. This makes PGO an interesting platform for tuning and designing different SOC effects in a way that complements the approach based on U-localisation and L-unquenching of half-filled valence bands depicted in ref. [65]. The localization of the bottom CB levels stems from the presence of natural empty channels and, along with the short-range character of the driving forces of the phase transition, supports ferroelectricity under n-doping conditions. Hence, the resulting design rule to obtain large SOC effects in crystals containing Pb²⁺ or Bi³⁺ cations would be to have them placed at the edge of a cavity to form unquenched 6p cavity states. This condition could potentially be explored in other materials with a similar crystal structure where natural empty channels are present, e.g. in $Pb_5(SiO_4)(VO_4)_2$ [66]. Exploiting the properties of the cavity-confined Pb 6p conduction orbitals would require photo-excitation techniques and/or doping, although alloving as well may be used as an exploratory method.

Being relatively confined, these wavefunctions may host novel and unexplored optoelectronic and quantum properties. If we assume a possible dependence on geometrical features, it would be interesting to further explore how the aforementioned states are affected by the size and the shape of the cavity enclosing them.

ACKNOWLEDGEMENTS

The authors acknowledge E. McCabe, Z. Romestan and S. Bandyopadhyay for fruitful discussions. Computational resources have been provided by the Consortium des Équipements de Calcul Intensif (CÉCI), funded by the Fonds de la Recherche Scientifique (F.R.S.-FNRS) under Grant No. 2.5020.11. MF & EB acknowledges FNRS for support and the PDR project CHRYSALID No.40003544. Work at West Virginia University was supported by the U.S. Department of Energy (DOE), Office of Science, Basic Energy Sciences (BES) under Award DE-SC0021375. We also acknowledge the computational resources awarded by XSEDE, a project supported by National Science Foundation grant number ACI-1053575. The authors also acknowledge the support from the Texas Advances Computer Center (with the Stampede2 and Bridges supercomputers). We also acknowledge the Super Computing System (Thorny Flat) at WVU, which is funded in part by the National Science Foundation (NSF) Major Research Instrumentation Program (MRI) Award #1726534, and West Virginia University.

^[1] J. Stöhr and H. C. Siegmann, <u>Magnetism: From Fundamentals to Nanoscale Dynamics</u> (Springer Berlin Heidelberg, Berlin, Heidelberg, 2006).

^[2] A. Manchon, J. Železný, I. M. Miron, T. Jungwirth, J. Sinova, A. Thiaville, K. Garello, and P. Gambardella, Rev. Mod. Phys. 91, 035004 (2019).

^[3] P. Gambardella and I. M. Miron, Phil. Trans. R. Soc. A 369, 3175 (2011).

^[4] Y. Tokura and N. Kanazawa, Chem. Rev. 121, 2857 (2021).

^[5] K. Everschor-Sitte, J. Masell, R. M. Reeve, and M. Kläui, J. Appl. Phys. 124, 240901 (2018).

^[6] A. Fert, N. Reyren, and V. Cros, Nat. Rev. Mater. 2, 17031 (2017).

^[7] M. Z. Hasan and C. L. Kane, Rev. Mod. Phys. 82, 3045 (2010).

^[8] X.-L. Qi and S.-C. Zhang, Rev. Mod. Phys. 83, 1057 (2011).

^[9] S. Murakami, N. Nagaosa, and S.-C. Zhang, Science 301, 1348 (2003).

^[10] J. Sinova, D. Culcer, Q. Niu, N. A. Sinitsyn, T. Jungwirth, and A. H. MacDonald, Phys. Rev. Lett. 92, 126603 (2004).

^[11] Y. K. Kato, R. C. Myers, A. C. Gossard, and D. D. Awschalom, Science 306, 1910 (2004).

^[12] B. A. Bernevig and S.-C. Zhang, Phys. Rev. Lett. 96, 106802 (2006).

^[13] J. D. Koralek, C. P. Weber, J. Orenstein, B. A. Bernevig, S.-C. Zhang, S. Mack, and D. D. Awschalom, Nature 458, 610 (2009).

^[14] M. P. Walser, C. Reichl, W. Wegscheider, and G. Salis, Nat. Phys. 8, 757 (2012).

^[15] A. Sasaki, S. Nonaka, Y. Kunihashi, M. Kohda, T. Bauernfeind, T. Dollinger, K. Richter, and J. Nitta, Nat. Nanotechnol. 9, 703 (2014).

^[16] L. L. Tao and E. Y. Tsymbal, Nat. Commun. 9, 2763 (2018).

^[17] L. L. Tao and E. Y. Tsymbal, J. Phys. D: Appl. Phys. 54, 113001 (2021).

^[18] E. Rashba, Sov. Phys.-Solid State 2, 1109 (1960).

^[19] Y. A. Bychkov and E. I. Rashba, J. Phys. C: Solid State Phys. 17, 6039 (1984).

^[20] D. Di Sante, P. Barone, R. Bertacco, and S. Picozzi, Adv. Mater. 25, 509 (2013).

^[21] L. L. Tao, T. R. Paudel, A. A. Kovalev, and E. Y. Tsymbal, Phys. Rev. B 95, 245141 (2017).

^[22] G. Dresselhaus, Phys. Rev. **100**, 580 (1955).

- [23] R. Moriya, K. Sawano, Y. Hoshi, S. Masubuchi, Y. Shi-raki, A. Wild, C. Neumann, G. Abstreiter, D. Bougeard, T. Koga, and T. Machida, Phys. Rev. Lett. 113, 086601 (2014).
- [24] H. Nakamura, T. Koga, and T. Kimura, Phys. Rev. Lett. 108, 206601 (2012).
- [25] M. Gmitra and J. Fabian, Phys. Rev. B 94, 165202 (2016).
- [26] F. Trier, P. Noël, J.-V. Kim, J.-P. Attané, L. Vila, and M. Bibes, Nat. Rev. Mater. 7, 258 (2022).
- [27] H. Djani, A. C. Garcia-Castro, W.-Y. Tong, P. Barone, E. Bousquet, S. Picozzi, and P. Ghosez, npj Quantum Materials 4, 51 (2019).
- [28] J. Hlinka, J. Privratska, P. Ondrejkovic, and V. Janovec, Phys. Rev. Lett. 116, 177602 (2016).
- [29] T. Hayashida, Y. Uemura, K. Kimura, S. Matsuoka, D. Morikawa, S. Hirose, K. Tsuda, T. Hasegawa, and T. Kimura, Nat. Commun. 11, 4582 (2020).
- [30] H. Iwasaki, K. Sugii, T. Yamada, and N. Niizeki, Appl. Phys. Lett. 18, 444 (1971).
- [31] H. Iwasaki, S. Miyazawa, H. Koizumi, K. Sugii, and N. Niizeki, J. Appl. Phys. 43, 4907 (1972).
- [32] See Supplemental Material at URL_inserted_by_publisher for more details concerning the computational details, structural information, PE frequency calculations, electronic properties, symmetry analysis, k·p model, P3 spin textures, Z₂ topological number and FE-PE barrier.
- [33] X. Gonze, F. Jollet, F. Abreu Araujo, D. Adams, B. Amadon, T. Applencourt, C. Audouze, J.-M. Beuken, J. Bieder, A. Bokhanchuk, E. Bousquet, F. Bruneval, D. Caliste, M. Côte, F. Dahm, F. Da Pieve, M. Delaveau, M. Di Gennaro, B. Dorado, C. Espejo, G. Geneste, L. Genovese, A. Gerossier, M. Giantomassi, Y. Gillet, D. Hamann, L. He, G. Jomard, J. Laflamme Janssen, S. Le Roux, A. Levitt, A. Lherbier, F. Liu, I. Lukačević, A. Martin, C. Martins, M. Oliveira, S. Poncé, Y. Pouillon, T. Rangel, G.-M. Rignanese, A. Romero, B. Rousseau, O. Rubel, A. Shukri, M. Stankovski, M. Torrent, M. Van Setten, B. Van Troeye, M. Verstraete, D. Waroquiers, J. Wiktor, B. Xu, A. Zhou, and J. Zwanziger, Computer Physics Communications 205, 106 (2016).
- [34] X. Gonze, B. Amadon, G. Antonius, F. Arnardi, L. Baguet, J.-M. Beuken, J. Bieder, F. Bottin, J. Bouchet, E. Bousquet, N. Brouwer, F. Bruneval, G. Brunin, T. Cavignac, J.-B. Charraud, W. Chen, M. Côté, S. Cottenier, J. Denier, G. Geneste, P. Ghosez, M. Giantomassi, Y. Gillet, O. Gingras, D. R. Hamann, G. Hautier, X. He, N. Helbig, N. Holzwarth, Y. Jia, F. Jollet, W. Lafargue-Dit-Hauret, K. Lejaeghere, M. A. Marques, A. Martin, C. Martins, H. P. Miranda, F. Naccarato, K. Persson, G. Petretto, V. Planes, Y. Pouillon, S. Prokhorenko, F. Ricci, G.-M. Rignanese, A. H. Romero, M. M. Schmitt, M. Torrent, M. J. van Setten, B. Van Troeye, M. J. Verstraete, G. Zérah, and J. W. Zwanziger, Computer Physics Communications 248, 107042 (2020).
- [35] M. Van Setten, M. Giantomassi, E. Bousquet, M. J. Verstraete, D. R. Hamann, X. Gonze, and G.-M. Rignanese, Comput. Phys. Commun. 226, 39 (2018).

- [36] J. P. Perdew, K. Burke, and M. Ernzerhof, Phys. Rev. Lett. 77, 3865 (1996).
- [37] J. P. Perdew, A. Ruzsinszky, G. I. Csonka, O. A. Vydrov, G. E. Scuseria, L. A. Constantin, X. Zhou, and K. Burke, Phys. Rev. Lett. 100, 136406 (2008).
- [38] G. Kresse and D. Joubert, Phys. Rev. B **59**, 1758 (1999).
- [39] K. Momma and F. Izumi, Journal of Applied Crystallography 44, 1272 (2011).
- [40] R. Viennois, I. Kityk, A. Majchrowski, J. Zmija, Z. Mierczyk, and P. Papet, Mater. Chem. Phys. 213, 461 (2018).
- [41] C. Konak, V. Kopsky, and F. Smutny, J. Phys. C: Solid State Phys. 11, 2493 (1978).
- [42] O. G. Vlokh, Ferroelectrics **75**, 119 (1987).
- [43] Y. Iwata, Journal of the Physical Society of Japan 43, 961 (1977).
- [44] R. Newnham, R. Wolfe, and C. Darlington, J. Solid State Chem. 6, 378 (1973).
- [45] R. Arras, J. Gosteau, H. J. Zhao, C. Paillard, Y. Yang, and L. Bellaiche, Phys. Rev. B 100, 174415 (2019).
- [46] S. C. Sabharwal, S. N. Jha, and Sangeeta, Bulletin of Materials Science 33, 395 (2010).
- [47] X. Wu, J. Xu, J. Xiao, A. Wu, and W. Jin, Journal of Crystal Growth 263, 208 (2004).
- [48] T. Rangel, D. Kecik, P. E. Trevisanutto, G.-M. Rignanese, H. Van Swygenhoven, and V. Olevano, Phys. Rev. B 86, 125125 (2012).
- [49] M. Hussain, M. Rashid, F. Saeed, and A. S. Bhatti, J. Mater. Sci. 56, 528 (2021).
- [50] M. S. Bahramy, R. Arita, and N. Nagaosa, Phys. Rev. B 84, 041202 (2011).
- [51] H. J. Zhao, H. Nakamura, R. Arras, C. Paillard, P. Chen, J. Gosteau, X. Li, Y. Yang, and L. Bellaiche, Phys. Rev. Lett. 125, 216405 (2020).
- [52] R. J. Elliott, Phys. Rev. **96**, 266 (1954).
- [53] Y. Yafet (Academic Press, 1963) pp. 1–98.
- [54] M. I. D'Yakonov and V. I. Perel', Soviet Journal of Experimental and Theoretical Physics 33, 1053 (1971).
- [55] B. A. Bernevig, J. Orenstein, and S.-C. Zhang, Phys. Rev. Lett. 97, 236601 (2006).
- [56] G. J. Omar, W. L. Kong, H. Jani, M. S. Li, J. Zhou, Z. S. Lim, S. Prakash, S. W. Zeng, S. Hooda, T. Venkatesan, Y. P. Feng, S. J. Pennycook, L. Shen, and A. Ariando, Phys. Rev. Lett. 129, 187203 (2022).
- [57] U. Herath, P. Tavadze, X. He, E. Bousquet, S. Singh, F. Muñoz, and A. H. Romero, Computer Physics Communications 251, 107080 (2020).
- [58] D. Gresch, G. Autès, O. V. Yazyev, M. Troyer, D. Vanderbilt, B. A. Bernevig, and A. A. Soluyanov, Phys. Rev. B 95, 075146 (2017).
- [59] A. A. Soluyanov and D. Vanderbilt, Phys. Rev. B 83, 235401 (2011).
- [60] Y. Wang, X. Liu, J. D. Burton, S. S. Jaswal, and E. Y. Tsymbal, Phys. Rev. Lett. 109, 247601 (2012).
- [61] F. Bruneval, C. Varvenne, J.-P. Crocombette, and E. Clouet, Phys. Rev. B 91, 024107 (2015).
- [62] P. Ghosez, X. Gonze, and J.-P. Michenaud, EPL 33, 713 (1996).
- [63] X. Gonze and C. Lee, Phys. Rev. B 55, 10355 (1997).
- [64] E. Bousquet and P. Ghosez, Phys. Rev. B 74, 180101 (2006).
- [65] J. Li, Q. Yao, L. Wu, Z. Hu, B. Gao, X. Wan, and Q. Liu, Nature Communications 13, 919 (2022).
- [66] S. Krivovichev, T. Armbruster, and W. Depmeier, Mater. Res. Bull. 39, 1717 (2004).